Si-waveguide-coupled Membrane InGaAsP-multiple-quantum-well Photodetector with Large Bandwidth at High Optical Input Power

Yoshiho Maeda, Tatsurou Hiraki, Takuma Aihara, Takuro Fujii, Koji Takeda, Tai Tsuchizawa, and Shinji Matsuo

NTT Device Technology Labs, NTT Corporation, 3-1 Morinosato-Wakamiya, Atsugi, Kanagawa 243-0198, Japan

E-mail: yoshiho.maeda.gk@hco.ntt.co.jp

Abstract: A Si-waveguide-coupled membrane photodetector (PD) with an InGaAsP multiple-quantum-well absorption layer shows a fiber-to-PD responsivity of 0.4 A/W and 3-dB bandwidth over 20 GHz at a fiber input power up to +5 dBm. © 2020 The Authors

1. Introduction

For sustainable growth of Internet traffic, issues that must be addressed are the cost, size, and power consumption of optical transceivers in datacenter network systems. A Si photonics platform has great potential as a solution because it enables us to integrate compact Si waveguide circuits on a silicon-on-insulator (SOI) wafer. On this platform, owing to the indirect bandgap of Si, lasers have been integrated by the direct bonding of direct-bandgap III-V semiconductors [1-3]. In such integrations, a recent approach has been to use the bonded III-V multiple quantum well (MQW) layer not only for the active region of the laser but also for the photodetector (PD) absorption region [4, 5]. This makes it possible to integrate waveguide-coupled PDs without additional epitaxial growth or bonding of bulk absorption layers, such as Ge or InGaAs, which is beneficial for reducing the fabrication cost of the optical transceivers.

However, a serious problem when we employ the MQW layer for the waveguide-coupled PD is electrical-field screening [6, 7]. In an MQW PD, electrical-field screening is observed at low input power because photo-generated carriers are well-confined in thin QW layers. Once electrical-field screening happens, the carrier transit time and junction capacitance increase significantly, resulting in degradation of the bandwidth. This poor input optical power tolerance is a critical problem in MQW PDs. Therefore, we have to reduce the absorption per unit length to where the carrier density in the MQW layer is low enough to suppress electric-field screening, which requires the increase of absorption length. As a result, we observe a bandwidth limitation due to large capacitance when we use a vertical *p-i-n* diode structure [7].

To overcome this problem, we propose a lateral membrane *p-i-n* diode with an InGaAsP MQW absorption layer, which is optically coupled with a Si waveguide. This structure enables us to achieve low capacitance due to its small cross-sectional area. To increase optical input power tolerance while maintaining a large bandwidth, we have to optimize the absorption per unit length by controlling the product of the optical confinement factor in absorption region, Γ, and absorption coefficient α. Γ is designed by changing the position and size of the Si waveguide, and α is controlled by changing the lateral electric field applied to the MQW layer. We fabricated a 300-μm-long waveguide PD using an MQW layer, which was used for a previous membrane laser diode [8], and demonstrated fiber-to-PD responsivity of 0.4 A/W and bandwidth of over 20 GHz with fiber input power of up to +5 dBm at wavelengths ranging from 1550 to 1600 nm. In addition, the fabricated device shows eye openings for 40-Gbit/s non-return-to-zero (NRZ) signals.

2. Design and fabrication

Figure 1(a) and (b) respectively show schematics of a bird's-eye view and cross section of the lateral MQW PD on the Si waveguide. The MQW core is buried in a 230-nm-thick InP layer, and a lateral *p-i-n* diode is formed. The photoluminescence peak wavelength of the MQW layer is 1520 nm, which is the same as that in our previous membrane laser diode lasing at around 1580 nm [8]. The MQW layer is optically coupled with a 220-nm-thick Si waveguide, and Γ in the MQW layer can be controlled thanks to the effective index matching between the membrane III-V and Si layers [8].

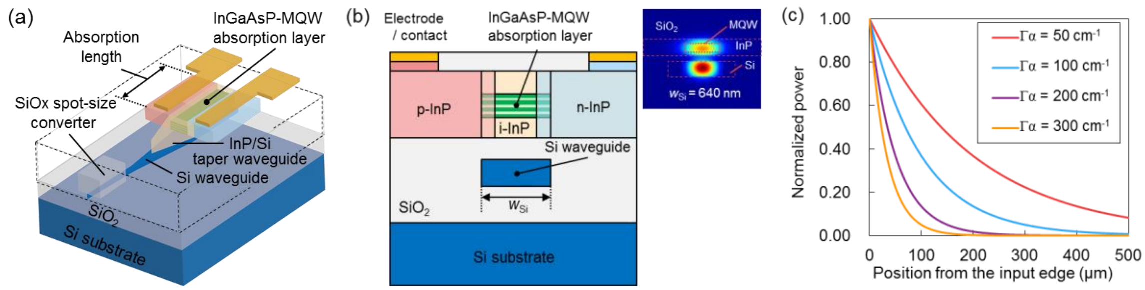

Fig. 1. (a) Bird's-eye view, (b) cross-sectional view of a Si-waveguide coupled membrane InGaAsP-MQW photodetector, and (c) $\Gamma\alpha$ dependence of absorption power distribution.

As described above, the key parameter is the product of the optical confinement factor Γ and absorption coefficient α of the MQW layer. Figure 1(c) shows calculated optical power in a waveguide PD with the $\Gamma\alpha$ of 50, 100, 200, and 300 cm^{-1}. In the calculation, we assumed that the optical supermode for III-V/Si is coupled to the input edge. As shown in the graph, the absorption per unit length decreases as the product of $\Gamma\alpha$ decreases, which results in improved input power tolerance. However, reducing $\Gamma\alpha$ requires a longer absorption length for high responsivity. Since the bandwidth of a waveguide PD is determined by its length, the bandwidth and optical input power tolerance are in a trade-off relationship.

Figure 2(a) shows the calculated capacitance and RC bandwidth of the proposed lateral membrane *p-i-n* diode. The membrane PD can achieve both a large bandwidth and high input power tolerance. In this work, we employed a 300-μm-long PD, which can be regarded as a lumped element and provides the bandwidth of around 27 GHz. This value is almost ten times larger than that of the conventional waveguide-coupled vertical *p-i-n* diode structure when they have the same absorption length. For this absorption length, $\Gamma\alpha$ is set to 100 cm^{-1}, so that 95% of incident light can be absorbed gradually over the entire length of 300-μm-long PD. Figure 2(b) shows confinement factors in the MQW layer, Si core, and p-InP region as a function of Si core width. As shown in this, Γ in the MQW layer decreases with increasing Si core width. It is also important to decrease Γ in the p-InP layer, which has large absorption loss. In this work, we set the core width to 640 nm, where the value of Γ in the MQW layer is 7.8% and Γ in the p-InP layer is small enough.

The device was fabricated on a SOI wafer as a following procedure. This process is compatible with that for the previously reported membrane laser [8]. First, a Si layer was patterned to form the Si waveguides, which was followed by deposition of a SiO_2 cladding film. After the SiO_2 surface had been polished, the MQW layer was bonded to the SOI wafer. The MQW layer was patterned to form a 600-nm-wide core and then buried in an InP layer by an epitaxial growth process. After that, donor and acceptor regions were formed by Si ion implantation and Zn thermal diffusion, respectively. Then the metal electrodes were fabricated. Finally, a 3-μm-square silica-based core was fabricated for low-loss fiber coupling [8]. Figure 2(c) shows the measured fiber-to-PD responsivity spectrum of the fabricated device in static operation. By increasing the reverse bias to the PD, α is increased by the Franz-Keldysh effect. As shown in Fig. 2(c), the target $\Gamma\alpha$ (100 cm^{-1}), where 95 % of incident light is absorbed, can be obtained by changing the DC biases from 2.0 V to 8.0 V for a ~50-nm optical bandwidth.

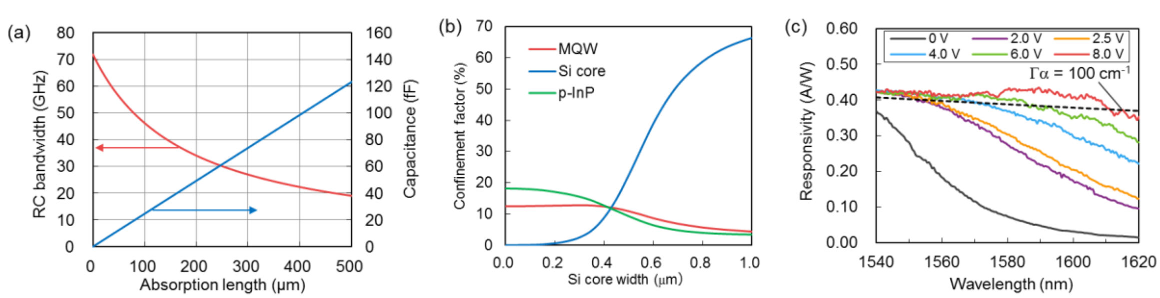

Fig. 2. (a) Absorption length dependence of RC bandwidth and junction capacitance, (b) a width of Si WG dependence of confinement factor on Si waveguide width, and (c) measured fiber-to-PD responsivity spectrum of 300-μm-long PD at each bias voltage.

3. Measured dynamic response

Figure 3(a) shows the measured frequency response of the fabricated device at a wavelength of 1550 nm and DC bias of 2.5 V. The fiber input power of -10 dBm was small enough to prevent electric-field screening. Thanks to the low capacitance, the measured 3-dB bandwidth was 25 GHz, which is over ten times larger than that of a typical 400-µm-long vertical *p-i-n* diode [7]. Figure 3(b) shows the fiber-input-power dependence of the 3-dB bandwidth at the wavelengths of 1550 and 1600 nm. The DC biases were 2.5 and 8.0 V, respectively. In these experiments, the input power of the modulated light was fixed to -10 dBm while the combined continuous light input power was increased. The maximum input power was +5 dBm, which was limited by the experimental setup. While slight carrier screening was observed at 1550 nm and 2.5 V, the measured bandwidths were over 20 GHz at fiber input power of up to +5 dBm at both wavelengths. Since the fiber-to-PD responsivity was 0.4 A/W, the photocurrent at +5-dBm input power was around 2 mA. Figure 3(b) also shows the measured 3-dB bandwidth at the wavelength of 1550 nm and DC bias of 8.0 V. Since $\Gamma\alpha$ was larger than its optimum value, the 3-dB bandwidth dramatically decreased with increasing input power over 0 dBm.

Finally, we measured eye diagrams for 40-Gbit/s non-return-to-zero (NRZ) signal. The fiber input power was 0 dBm, which was limited by our experimental setup. The input modulated optical signal was launched by a commercially available lithium niobite Mach-Zehnder modulator and coupled to the fabricated device by a lensed fiber. The photocurrent was measured with an RF probe then fed into a sampling oscilloscope. Figure 3(c) and (d) show the measured eye diagrams at wavelengths and of 1550 and 1600 nm and DC biases of 2.5 and 8.0 V, respectively. We obtained the eye opening at 40 Gbit/s thanks to the bandwidth of over 20 GHz.

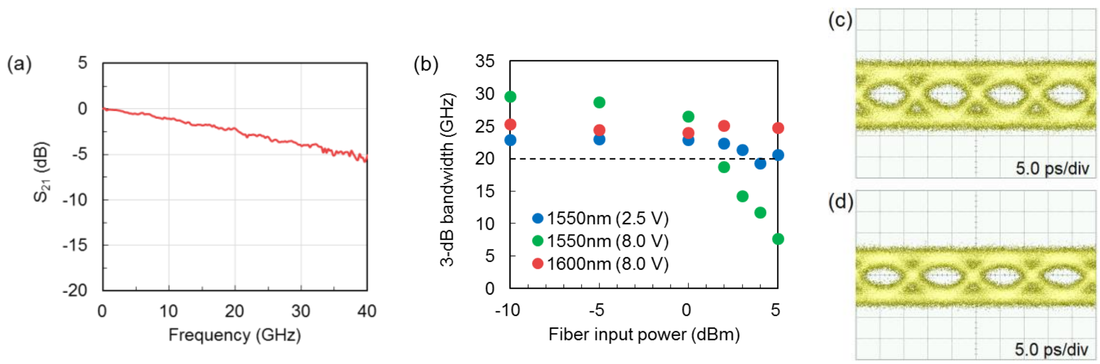

Fig. 3. (a) Measured frequency response at wavelength of 1550 nm, (b) fiber input power dependence of 3-dB bandwidth at wavelengths of 1550 nm and 1600 nm, and measured eye diagrams for NRZ with 40 Gbit/s at wavelengths of (c) 1550 nm and (d) 1600 nm, respectively.

4. Conclusion

We demonstrated a 300-µm-long membrane InGaAsP-MQW PD on a Si waveguide. Thanks to its coupling scheme for optimum optical confinement, the PD shows a fiber-to-PD responsivity exceeding 0.4 A/W in the wavelength range of 1550-1600 nm and a bandwidth of over 20 GHz at a fiber input power of up to +5 dBm. We also showed the eye opening at 40 Gbit/s NRZ signal. The use of an active MQW layer for the PD absorption layer is promising for reducing the cost of optical transmitters and fabricating large-scale photonic integrated circuits on a Si platform.

5. References

[1] A. W. Fang, *et. al.*, "Electrically pumped hybrid AlGaInAs-silicon evanescent laser," Opt. Exp. **14.20**, 9203-9210 (2006).

[2] S. Matsuo, *et. al.*, "Directly modulated buried heterostructure DFB laser on SiO_2/Si substrate fabricated by regrowth of InP using bonded active layer," Opt. Exp. **22**, 12139-12147 (2014).

[3] T. Fujii, *et. al.*, "1.3-µm directly modulated membrane laser array employing epitaxial growth of InGaAlAs MQW on InP/SiO_2/Si Substrate," in *European Conference on Optical Communication* (ECOC, 2016) PDP, Th.3.A.2.

[4] H. Park, *et. al.*, "A hybrid AlGaInAs-silicon evanescent preamplifier and photodetector," Opt. Exp. **15,** 13539-13546 (2007).

[5] Y. Baumgartner, *et. al.*, "Novel CMOS-Compatible Ultralow Capacitance Hybrid III-V/Si Photodetectors Tested up to 32 Gbps NRZ," in *Optical Fiber Communication Conference* (OFC, 2019), Th3B.3.

[6] T. H. Wood, *et. al.*, "Electric field screening by photogenerated holes in MQWs: A new mechanism for absorption saturation," Appl. Phys. Lett. **57.11,** 1081-1083 (1990).

[7] H. Park, *et. al.*, "A hybrid AlGaInAs-silicon evanescent waveguide photodetector," Opt. Exp. **15.10,** 6044 (2007).

[8] T. Aihara, *et. al.*, "Lateral current injection membrane buried heterostructure lasers integrated on 200-nm-thick Si waveguide," in *Optical Fiber Communication Conference* (OFC, 2018) W3F.4.